The Mechanism for Low-pH-Induced Clustering of Phospholipid Vesicles Carrying the HA2 Ectodomain of Influenza Hemagglutinin†

Chul-Hyun Kim, Jed C. Macosko, and Yeon-Kyun Shin*

Department of Chemistry, University of California, Berkeley, California 94720

Received August 11, 1997; Revised Manuscript Received October 29, 1997⊗

ABSTRACT: Homotrimeric hemagglutinin (HA) is one of the major spike membrane glycoproteins of the influenza virus. Initial pH-triggered conformational changes in the target membrane-interacting HA2 domain are necessary for a preliminary step in membrane fusion. Using spin-labeling electron paramagnetic resonance (EPR) spectroscopy, we examined subsequent pH-dependent changes of a membrane-bound HA2 construct (FHA2, aa 1−127). Residues 91−94, 108−115, 122, and 125 were mutated to cysteine and spin-labeled. Low solvent accessibility and side chain mobility were observed by EPR at positions 91−94, 122, and 125. Spin-labels at residues 108−115 were solvent-exposed and highly mobile, revealing the presence of a flexible loop. These results are consistent with the low-pH crystal structure of a truncated HA2 domain, particularly the unusual kink loop at residues 108−115 [Bullough et al. (1994) *Nature (London) 371*, 37−43]. Most interestingly, at endosomal pH, spin-labels at 108−115 become immobile and no longer solvent-exposed, and this change is reversible upon reneutralization. However, little change in the EPR line shape and accessibility of spin-labels was observed in other regions. This observation implies that the FHA2 trimers interact reversibly via this specific loop, most likely in an intermolecular fashion. Furthermore, this interaction correlates well with a reversible pH-dependent clustering of FHA2-bearing vesicles evidenced by the reversible increase in turbidity and further confirmed in detail by electron microscopy. The implications of this reversible, pH-dependent interaction between FHA2 trimers are discussed in light of recent fusion models.

Membrane fusion is an integral step in many fundamental biological processes, including viral infection, synaptic transmission, fertilization, and intracellular protein trafficking (reviewed by *1*). Specialized proteins are required for most of these processes (for review, see *2*). In an effort to elucidate mechanisms of protein-mediated membrane fusion, the hemagglutinin (HA) of the influenza virus is valuable as the best characterized membrane fusion protein. Its clinical importance as well as its fundamental biological interest as a model system for fusion has contributed to the extensive research on HA during the past few decades.

Hemagglutinin (HA) is one of the major membrane spike proteins of the influenza virus. Viral infection begins with the binding of HA to sialic acid-containing receptors on the surface of the target cell. Following receptor-mediated endocytosis of the virus *(3)*, HA mediates the fusion of the viral membrane with the endosomal membrane, enabling the passage of the viral genome into the host cytoplasm. A key step in triggering this fusion process is a conformational change of HA from the native state to the fusogenic state *(4)*. This transition is triggered by the mildly acidic pH in the mature endosome (for review, see *5* and *6*).

In the native state, HA is a homotrimer consisting of two subunits, the receptor-binding HA1 domain and the membrane-interacting HA2 domain *(7)*. The crystal structure of the ectodomain HA at neutral pH indicates that the HA2 domain consists of an essential fusion peptide in the NH_2-terminal region, a short α-helix, a hairpin loop, and a long helical stem in the COOH-terminal region which protrudes from the viral membrane (Figure 1A). Three such long helices assemble into a three-stranded coiled-coil to form the core of the HA homotrimer. One interesting feature of the native HA structure is that the target membrane-interacting fusion peptide is tucked inside the protein, nearly 100 Å away from the top of the molecule.

Previous studies have shown that under mildly acidic conditions, HA1 is partially dissociated from HA2 and the hydrophobic fusion peptide is exposed to the aqueous phase, enabling its interaction with the target membrane *(4, 8−10)*. The question arises as to how this fusion peptide interacts with the distal endosomal membrane.

Recently, one model based on structural predictions hypothesizes a global conformational change *(11)*. The model proposes that the hairpin loop region in the neutral pH crystal structure of HA2 (Figure 1A) undergoes a drastic conformational change to a long coiled-coil at low pH (Figure 1B), thereby extending the trimeric stem and allowing relocation of the fusion peptide toward the top of the ectodomain. The low-pH X-ray crystal structure of the soluble HA2 domain (TBHA2, *12*) added further evidence for the proposed pH-dependent loop-to-helix transition. This structure is a major advance in understanding the initial step of membrane fusion. Yet, little is known about what happens

† This work was supported by a Searle Scholarship to Y.-K.S.

* To whom correspondence should be addressed. Telephone: (510) 643-5507. Fax: (510) 643-1255. E-mail: shin@cchem.berkeley.edu.

⊗ Abstract published in *Advance ACS Abstracts,* December 15, 1997.

S0006-2960(97)01982-X CCC: $15.00
Published on Web 01/06/1998

after the fusion peptide binds to the target membrane. The fundamental question is: How does HA mediate membrane apposition and fusion?

Interestingly, the low-pH crystal structure of the soluble HA2 construct indicates that the long coiled-coil stem of the pH 7 structure breaks into a kinked motif with a flexible loop in the turn of the kink (Figure 1B). A similar structural rearrangement has also been observed for HIV gp41 *(13, 14)* and the transmembrane (TM) subunit of Moloney murine leukaemia virus (MoMuLV) (15). This gives rise to an important question: What is the physiological importance of this unexpected structural motif? To elucidate the functional role of the kink in triggering membrane fusion and to correlate it with other fusion mechanisms, a spin-labeling EPR study on the stem region has been performed using a membrane-reconstituted HA2 construct (FHA2, aa 1−127) containing the fusion peptide and the coiled-coil stem region.

We found that the kinked loop residues (black loop in Figure 1B) interact with one another at low pH. Other residues in the stem region appear not to interact. Furthermore, the structure of the fusion peptide region as well as the hairpin-loop region (dark gray in Figure 1B) of the membrane-bound HA2 has been investigated recently using spin-labeling EPR, and negligible pH-dependent conformational change was found in these regions upon acidification *(16, 17)*. The lack of pH-dependent change in other regions suggests that interactions between HA2 trimers in the membrane fusion process are mediated through the kinked region of HA2. After reporting on the pH dependence of the kinked region, we examine its implications for recently proposed models of HA-induced membrane fusion.

MATERIALS AND METHODS

Materials. FHA2 and its site-specific cysteine mutant proteins were all expressed in *E. coli*. The strain used for expression of plasmids bearing FHA2 was *E. coli* BL21-(DE3) pAcyc [*hsdS gal* (λcIts857 *ind* 1 Sam7 *nin* 5 *lac* UV5-T7 gene*1*)]. The original gene for the soluble part of the HA2 domain (SHA2, aa 33−127) was kindly provided by Dr. Peter S. Kim at MIT. SHA2 was expressed in *E. coli* BL21(DE3) using the original vector. The NH_2-terminal region (aa 1−32) was inserted onto the original gene, and for overexpression and site-specific mutagenesis, we subcloned it into the pET 21a(+) plasmid vector which was purchased from Novagen (Madison, WI). For plasmid purification and amplification, we used the *E. coli* strain DH5α [*sup*E44 Δ*lac* U169 (*ϕ*80 *lac* ZΔM15) *hsd* R17 *rec* A1 *end* A1 *gyr* A96 *thi* −1 *rel* A1]. For single-strand DNA preparation, we used the *E. coli* strain CJ236 [*dut* 1 *ung* 1 *thi* -1 *rel* A1/pCJ105(cam^r F')]. Isopropyl β-D-thiogalactopyranoside (IPTG) was purchased from United States Biochemical (Cleveland, OH). *n*-Octyl β-D-glucoside (OG) was purchased from Anatrace (Maumee, OH). Triton X-100 was purchased from Fisher Scientific (Fair Lawn, NJ). 1-Palmitoyl-2-oleoylphosphatidylcholine (POPC) and 1-palmitoyl-2-oleoylphosphatidylglycerol (POPG) were purchased from Avanti Polar Lipids (Birmingham, AL). *S*-(1-Oxy-2,2,5,5-tetramethylpyrroline-3-methyl)methanethiosulfonate (MTSSL) spin-label was from Reanal (Hungary), and [α-^{35}S]dATP was from Amersham (Arlington Height, IL). Q-Sepharose fast flow resin and DEAE Sepharose fast flow resin were purchased from Pharmacia Biotech (Uppsala, Sweden).

Expression and Purification of FHA2. FHA2 and its site-specific cysteine mutant proteins were all expressed and purified from *E. coli*, using the materials and protocol described previously *(17)*. The original gene was designed to express a soluble construct of HA2 (SHA2, aa 33−127). We extended this construct to include the fusion peptide region (FHA2, aa 1−127). For purification, 5 mM citrate−phosphate buffer (pH 7.0) which contains 1 mM EDTA, 1 mM phenylmethanesulfonyl fluoride (PMSF), 4 mM DTT, 150 mM NaCl, and 0.5% Triton X-100 was used. The purity achieved was higher than 95%, and the net protein yield was approximately 3−4 mg/1.5 L of culture.

Expression and Purification of SHA2. SHA2, the original construct of the soluble HA2 domain (aa 33−127), was expressed in *E. coli* BL21(DE3) using M9 ZB media *(18)* with the same IPTG induction protocol as for FHA2. After breaking cells, the crude extract was spun down at 10000*g*, and the supernatant was taken to be precipitated with different concentrations of ammonium sulfate (50% and 80%). Using the desalting column, ammonium sulfate was removed, and the protein was purified through a Q-Sepharose column using a NaCl gradient (80−500 mM). The purified fractions were further purified through a DEAE Sepharose column using the same NaCl gradient. The final purity was about 95%.

Site-Directed Mutagenesis. In the full-length HA2 domain, there are several native cysteines; however, none exist in residues 1−127. Cysteine mutants of FHA2 were generated using the method described by Kunkel *(*ref *19)*. Figure 2A shows mutation sites in FHA2 (aa 91−94, 108−115, 122, and 125). In SHA2, residues 64 and 113 were also mutated to cysteine. DNA sequences of the wild type and all mutants were confirmed by DNA sequencing using the Sequenase Version 2.0 DNA sequencing kit (United States Biochemical, Cleveland, OH).

Vesicle Preparation and Reconstitution. Uniformly-sized lipid vesicles (100 nm in diameter) containing 80 mol% 1-palmitoyl-2-oleoylphosphatidylcholine (POPC) and 20 mol% 1-palmitoyl-2-oleoylphosphatidylglycerol (POPG) were made as previously described *(20)*. For reconstitution, the vesicle solution was perturbed by 0.5% (final concentration) *n*-octyl β-D-glucoside (OG), and mixed with Triton X-100-solubilized FHA2 mutants or with OG-solubilized FHA2 mutants (H64C and Q65C). The final concentration of lipid in the mixture was 10 mM, and the protein concentration was 10 μM (1:1000 molar ratio of protein to lipid). The detergent was removed with Bio-Bead SM2 resin (BioRad, Hercules, CA) following a column protocol *(21)*. The unreconstituted protein aggregate was then removed by high-speed centrifugation (10000*g*). Finally, the reconstituted vesicles were pelleted and resuspended following our previous protocol *(16)*.

Site-Specific Spin-Labeling EPR. EPR measurements were performed at 37 °C (for greater physiological relevance) using a Bruker ESP 300 EPR spectrometer (Bruker, Germany) equipped with a low-noise microwave amplifier (Miteq, Hauppauge, NY) and a loop-gap resonator (Medical Advances, Milwaukee, WI). The modulation amplitude was set at no greater than one-fifth of the line width. All the

cysteine mutants were labeled with MTSSL spin-label and quantified according to prior methods *(17)*. For all mutants examined, the spin-labeling ratios were nearly quantitative.

EPR Accessibility Measurement. Nitroxide accessibility was measured using the power saturation technique described previously *(22, 16)*. NiEDDA was generously provided by Dr. Wayne Hubbell at UCLA and used at a final concentration of 10 mM. This concentration is lower than that (200 mM) in our previous study of the membrane-inserted fusion peptide region *(16)* because the low concentration was necessary for distinguishing differences in solvent accessibility for the primarily aqueous stem region. The accessibility parameter W_A (in units of milliwatts per gauss), which is proportional to the Heisenberg spin exchange rate, is obtained from $\Delta P_{1/2}/\Delta H^*$. $\Delta P_{1/2}$ is the difference between $P_{1/2}$ values in the presence and in the absence of a relaxing reagent. $P_{1/2}$ is the microwave power where the first-derivative amplitude is reduced to the half of its unsaturated value. ΔH^* is the peak to peak line width of the $M_I = 0$ EPR line.

Altering the pH of Reconstituted FHA2. To lower the pH, we added 100 mM sodium acetate buffer (pH 5.0) to the reconstituted FHA2 sample (resuspended in 5 mM citrate−phosphate buffer, pH 7.0) at a volume ratio of 1:4. To return the pH to neutral, we added 1 M Tris, pH 7.0, to the pH 5 sample at a volume ratio of 1:4.

Electron Microscopy. The FHA2-reconstituted phospholipid vesicles were observed at pH 7, at pH 5, and after reneutralization using a Zeiss EM10 Transmission Electron Microscope (Carlzeiss Inc., Germany). Since the staining procedure could alter the pH and disturb the original state of the vesicles (uranyl acetate staining solution is acidic), we chose not to stain the FHA2-reconstituted vesicles.

RESULTS

Generation of FHA2 Cysteine Mutants for Nitroxide-Scanning EPR. In this study, we used a polypeptide derived from the essential components of HA2 (FHA2: aa 1−127), including the hydrophobic fusion peptide at the N-terminus and the entire helical stem at the C-terminus (Figure 1). FHA2 is a trimeric protein, as is intact HA *(17)*. When reconstituted into phospholipid vesicles, the N-terminal fusion peptide region was found to be imbedded in the bilayer as monomeric helices at an oblique angle *(16)*, while the long coiled-coil region remains in solution with substantial flexibility *(17)*. Most probably, reconstituted FHA2 mimics an early HA2 intermediate in the fusion process subsequent to the initial fusogenic conformational change and the binding of the fusion peptide to the membrane. The structure of the stem region of FHA2 in the membrane-bound state was investigated using nitroxide-scanning EPR experiments. For these experiments, thiol-specific nitroxide spin-labels were attached to a unique cysteine residue site in each FHA2 mutant. We prepared 14 novel cysteine mutants covering the upper part of the stem (L91C, W92C, S93C, Y94C), the kinked loop (I108C, D109C, L110C, T111C, D112C, S113C, E114C, M115C), and the end of the stem (T122C, Q125C). We also examined two previously generated cysteine mutants of the hairpin-loop region (H64C and Q65C) for comparison. A schematic diagram for all the new mutation sites is shown in Figure 2A.

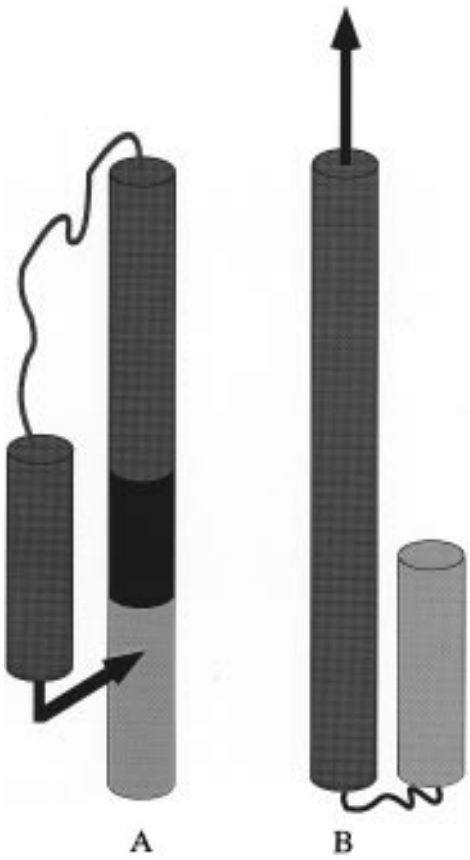

FIGURE 1: Schematic structural models showing the core structural change of an HA2 monomer at (A) pH 7 and (B) pH 5. The fusion peptide (aa 1−25) is shown as a black arrow, in dark gray is the central helix involved in the trimeric long coiled-coil (aa 38−104), in black the bunching kink (aa 105−113), and in light gray the buttressing helix (aa 114−127). Cylinders represent α-helices.

Spin-Labeling EPR at Neutral pH. The stem domain of FHA2 was examined using EPR spectroscopy. The EPR spectra of spin-labeled FHA2 mutants are shown in Figure 2B. Generally, EPR spectra are sensitive to the local structure. For instance, if the nitroxide side chain is attached to a flexible loop exposed to the solution phase, a fast motional, therefore sharp, line shape is expected. On the other hand, if the nitroxide is in tertiary contact with a neighboring structure, a broad spectrum is expected due to a more retarded motion. Furthermore, since spectra are affected by the proximity of neighboring nitroxides, when a nitroxide is attached to an internal position of a coiled-coil, an "exchange-broadened" EPR spectrum is expected due to the spin exchange interaction between clustered nitroxides *(17)*.

Careful examination of EPR line shapes revealed a flexible loop region spanning eight residues from I108C to M115C. EPR spectra of spin-labeled T111C through E114C (Figure 2B) are all relatively sharp (2−3 G line width of the central, $m_I = 0$, resonance) with no sign of strong spin exchange interactions, which indicate relatively fast motional nitroxides such as those attached to a flexible solvent-exposed loop *(23)*. EPR spectra of I108C through L110C and M115C are relatively broader, consistent with the reduced motion near the ends of a loop.

Furthermore, the accessibility of water-soluble paramagnetic nickel ethylenediaminediacetic acid (NiEDDA) to the

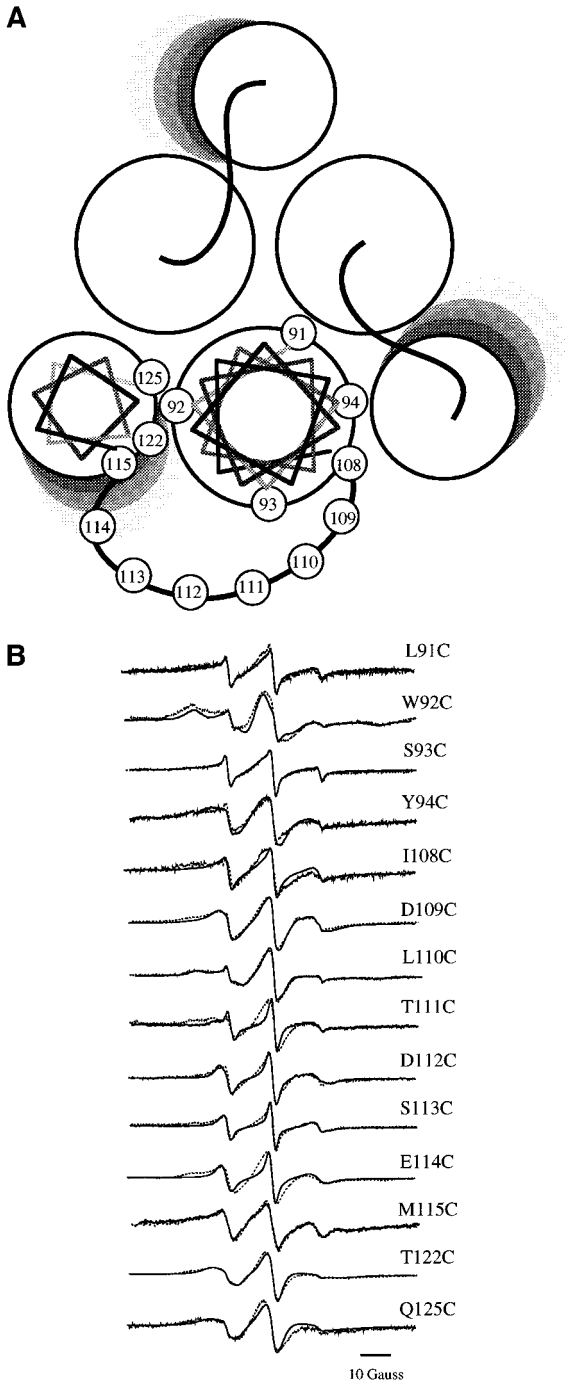

FIGURE 2: (A) Diagram based on the low-pH crystal structure *(12)* of the FHA2 stem region looking down the trimer axis from the kinked region. Mutation sites used in this study are shown in only one monomer for clarity. The tilt in the buttressing helices is shown by shaded disks. (B) EPR spectra of the 14 FHA2 mutants used in this study at pH 7 (solid lines) and pH 5 (broken lines). The broadening in the spectra for T111C, D112C, S113C, and E114C is clearly visible.

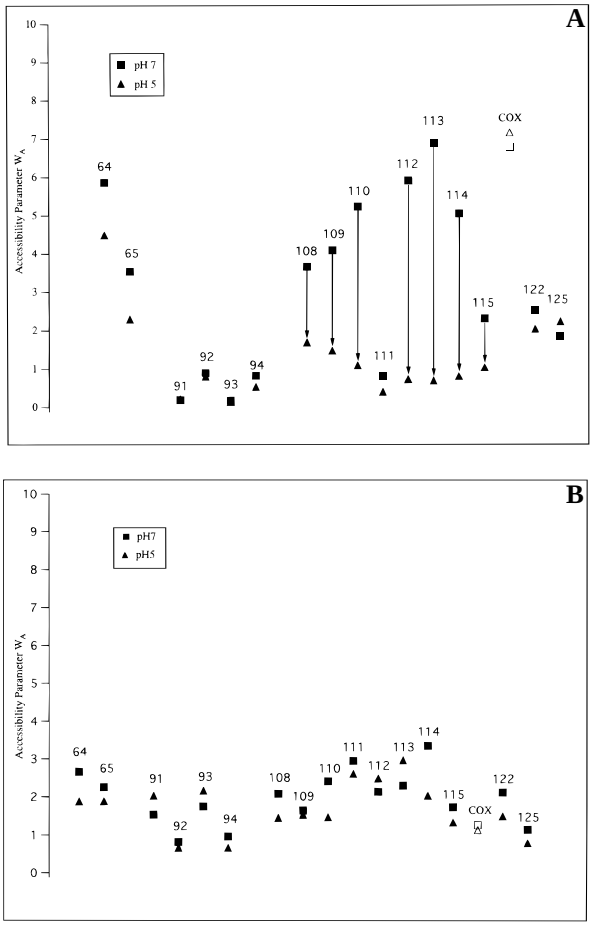

FIGURE 3: Accessibility parameter, W_A, for FHA2 mutants at pH 7 and 5 in (A)10 mM NiEDDA and (B) ambient O_2. These values reflect the amount of accessibility of the particular paramagnetic agent to the spin-labeled residue indicated. A large pH-dependent change in accessibility is observed for residues 109−114. This change is interpreted as evidence for a bunching of FHA2 molecules at this region. A well-characterized soluble peptide, the 25-residue signal peptide from yeast cytochrome C oxidase subunit IV (COX), shown in open symbols, was used as the standard value of W_A for a fully exposed case *(24)*. The change in accessibility was negligible between pH 7 and pH 5 for COX in either NiEDDA or O_2. This confirmed that the change of the accessibility parameter is not generally affected by pH unless the change triggers some structural rearrangement.

nitroxides attached to residues in this loop region has been measured using EPR saturation techniques (Figure 3A). This accessibility parameter has been previously found to be directly proportional to the solvent-accessible area of the residue (W. Hubbell, personal communication). When compared with the high accessibility of a fully exposed nitroxide attached to a well-characterized test peptide, the 25-residue signal peptide from yeast cytochrome C oxidase subunit IV (COX, ref *24*), all nitroxides from I108C to M115C except T111C also show high accessibility. This implies that they are nearly fully exposed, again consistent with an aqueous loop-like structure. S113C, in the middle of the loop, has the highest accessibility, nearly the same as the COX peptide. A decrease in accessibility has been observed for the residues closer to the end of the putative loop. The hairpin-loop region (H64C and Q65C) showed high accessibility comparable with both the highly exposed positions of the kinked region and the COX peptide.

In contrast, motionally slow, broadened EPR spectra of nitroxides attached to the upper part of the stem domain (L91C−Y94C) at pH 7 might be consistent with a coiled-coil structure (Figure 3B). Spin-exchange broadening has been observed for Y94C (and to some extent for L91C) as evidenced by the line broadening further to the low field and to the high field, which can be better seen in the integrated absorption spectrum (data not shown). These

findings are again consistent with spin-labels at internal coiled-coil positions. Furthermore, EPR spectra of the end region (T122C and Q125C) are motionally broadened but not spin−spin-interacting, and correspond well with a buttressing helical structure (light gray, Figure 1B). In addition, NiEDDA accessibility of the upper stem region at pH 7 is conspicuously low (Figure 3A), also implying that the residues are buried through coiled-coil and buttressing-helix tertiary interactions.

For membrane-reconstituted FHA2 at neutral pH, EPR line shapes as well as accessibility data are fully consistent with the low-pH crystal structure. Such consistency in this membrane-bound FHA2 construct lends support to the claim that the low pH conformation is a thermodynamically stable structure of membrane-bound HA2 at neutral pH in the absence of HA1. This claim would imply that the HA conformational change to the fusogenic state (Figure 1) is indeed kinetically controlled *(11)*.

Spin-Labeling EPR at Low pH. Upon lowering the pH from 7 to 5, we have observed significant changes in NiEDDA accessibility in the kinked region of FHA2 (Figure 3A). A significant decrease in accessibility for each nitroxide was observed in this loop with the exception of T111C which appeared to be affected by the cysteine mutation such that the accessibility at pH 7 was already very low. The dramatic decrease in accessibility indicates that this region becomes much less exposed to the solvent under low-pH conditions. Most conspicuously, the nitroxide at position 113 in the middle of the loop which was as exposed as the COX peptide at pH 7 became nearly fully protected from the collision with NiEDDA at pH 5. Furthermore, as shown in Figure 2B, the EPR line shapes become broader at low pH due to both retarded motion and some spin−spin interactions at positions 108 through 114. These spin−spin interactions suggest that the nitroxide attached at the loop makes contact with another nitroxide-bearing loop of a second FHA2 molecule. The accessibility data and the EPR line broadening together strengthen the hypothesis that the kinked loops of one FHA2 trimer interact with the same region on another FHA2 trimer.

Moreover, a significant pH-dependent change in neither EPR line shape nor the accessibility to NiEDDA has been observed for nitroxides attached to L91C through Y94C and for T122C and Q125C. Although there is some decrease in accessibility on the hairpin loop region (H64C and Q65C), this change is not as conspicuous as for the kinked region. Considering the previous results which showed little pH-dependent change in EPR line shapes on the hairpin loop region *(17)* and the fusion peptide region *(16)*, our results imply that the intermolecular interaction between FHA2 trimers is localized and mediated primarily through the interaction between kinked loops.

However, it is still possible that the pH-dependent change in accessibility and EPR line shape is due to the insertion of the kinked loop into the membrane bilayer. By examining the accessibility to nonpolar oxygen molecules (O_2), we could better discern whether the EPR changes were due to the interaction between loops of FHA2 trimers or to the interactions of the loops with the bilayer *(25)*. The concentration of O_2 inside the nonpolar bilayer is as much as 10 times higher than it is in the aqueous phase. If the kinked loop regions were to interact with the lipid bilayer upon acidification, a significant increase of collision with O_2 would have been expected for nitroxides in this region. The accessibility to O_2 for all nitroxides in this region at neutral pH is similar to that of the solution-exposed COX peptide, and no significant pH-dependent change has been observed for any nitroxide (Figure 3B). These results rule out the possibility of membrane insertion for the kinked region. Thus, the extensive EPR line broadening and the protection from the solvent at low pH seem indeed likely to stem from direct intermolecular loop to loop interactions between FHA2 trimers.

We must keep in mind, however, that our interpretation is based on the assumption that the overall structure of FHA2 remains unchanged as the pH is lowered. It is possible that the kink undergoes an intramolecular structural rearrangement at low pH which sequesters the kink and then triggers an intermolecular FHA2 clustering. Yet, the lack of observable structural rearrangements in any other region except the kinked region makes this possibility seem unlikely.

pH-Dependent Reversible Clustering of Vesicles Containing FHA2. In addition to microscopic phenomenon, the macroscopic effects of low-pH on FHA2 could also provide important insight into the subsequent steps of membrane fusion. We found that the macroscopic evidence of a pH-dependent change was a significant turbidity increase at pH 5 in vesicles carrying FHA2 (Figure 4A). Since all possible nonspecific protein aggregates were removed in the reconstitution process and vesicles without FHA2 did not show any change in turbidity at low pH, this change in the turbidity must be related to a change in vesicles induced by FHA2. We also found that this change was reversed upon readjusting the pH to 7 (Figure 4A). This reversibility weakens the possibility that the pH-dependent turbidity change was due to an increase of the vesicle size through FHA2-induced fusion, since membrane fusion is an irreversible process. Therefore, the turbidity change is most likely due to the clustering of vesicles and is induced by FHA2 molecules on their surface. Although this clustering is not the same as fusion, understanding its molecular mechanism could be a key to understanding the functional role of the stem region in HA2 activation as well as in subsequent steps of membrane fusion.

EPR accessibility experiments and line shape analyses would suggest that the kink region is responsible for the macroscopic clustering of vesicles. Since the clustering is reversible, we should then expect identical reversibility in the EPR broadening of the kinked region if these observations are directly correlated. Indeed, for all spin-labeled mutants, we found that, after a pH cycle from 7 to 5 to 7, the EPR spectra returns to its initial line shape. An example of the reversible change for S113C is shown in Figure 5. This close match in reversibility between the macroscopic change in turbidity and the microscopic changes in the EPR spectra of the kink region is consistent with the idea that the protein−protein interaction in the kinked region is the molecular level mechanism for FHA2-induced vesicle clustering. Although reversible pH-dependent clustering of vesicles is not the same process as pH-dependent membrane fusion, the interacting tendency of the kink may have profound implications as models for HA-mediated membrane fusion are developed.

Electron Microscopic Observation. Electron microscopy (EM) provides an ideal bridge between microscopic and macroscopic observations. We used EM to verify the

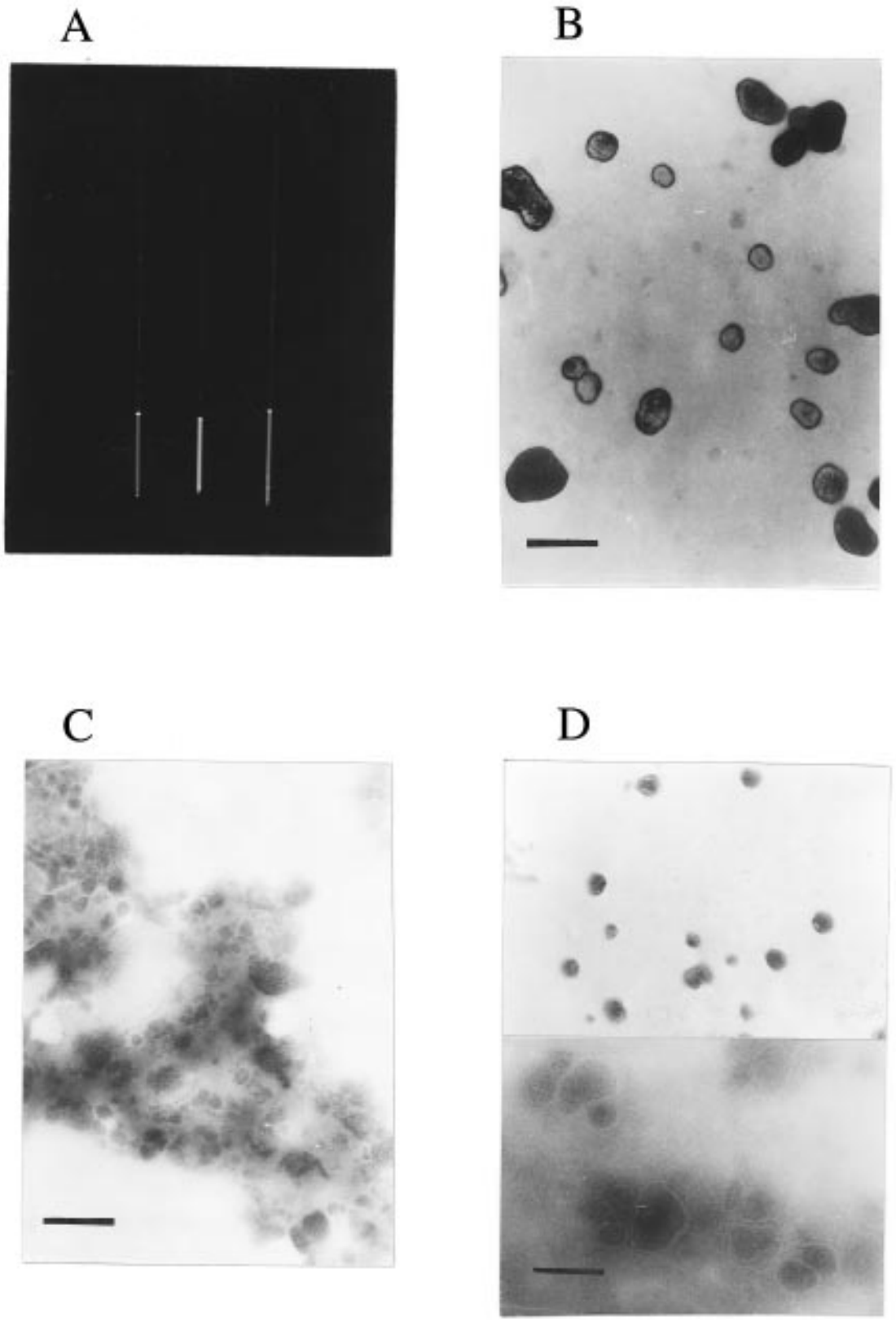

FIGURE 4: (A) Photograph of three capillaries containing FHA2 bound to lipid vesicles under different conditions: (left) in pH 7 buffer, (middle) in pH 5 buffer, (right) in pH 7 buffer after incubation at pH 5 for 10 min at 37 °C. The decrease in light scattering from middle to right indicates that vesicles cluster together reversibly at pH 5. Although the total volume loaded into each capillary was different, the concentrations were all equivalent. (B) Electron micrograph of FHA2 (36000× magnification) bearing vesicles at pH 7, (C) pH 5, and (D) pH 7 after incubation for 10 min at pH 5. (B) and (D) show dispersed vesicles whereas in (C) the vesicles are highly clustered. Bars indicate 300 nm.

presence of FHA2-containing vesicle clusters at pH 5. As shown in Figure 4B−D, vesicles containing FHA2 are dispersed at pH 7, become highly clustered at pH 5, and then return to a more disperse state upon reneutralizing the pH. In Figure 4B, both single vesicles and clusters of few vesicles can be seen. This situation is quite different from

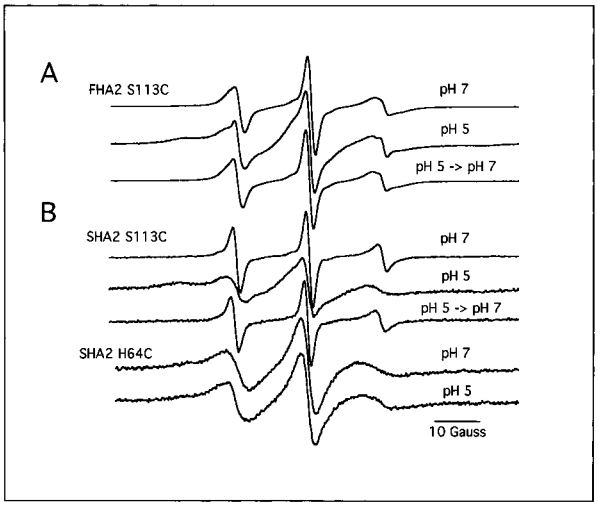

FIGURE 5: (A) EPR spectra for FHA2 S113C demonstrating the reversibility of the FHA2 pH-dependent broadening. (B) EPR spectra for SHA2 mutants. SHA2 S113C shows a similar reversible broadening as in FHA2 whereas H64C does not change with pH.

the state at pH 5 shown in Figure 4C. In this case, many of the vesicles appear to be clustered together. At the edges of the clusters, individual vesicles can be seen, which is further evidence that the vesicles cluster but do not fuse. After reneutralization, there are no longer any large clusters visible; however, it appears that some of vesicles are not yet completely dissociated. The upper panel of Figure 4D shows a region of the reneutralized sample where vesicles are disperse. The lower panel is an example of a more clustered region which is not fully dissociated. Even in this clustered region, the average number of vesicles is less than 10, more than an order of magnitude fewer than at pH 5. The clear evidence of clustering at pH 5 and the relatively dispersed nature of vesicles at pH 7 supports the hypothesis that macroscopically observed turbidity is due to reversible vesicle clustering. This clustering in turn implies that FHA2 exhibits pH-dependent intermolecular protein−protein interactions.

Spin-Labeling EPR on the Soluble HA2. As further evidence that the changes in the kinked region are due to protein−protein interactions and not because of nonspecific protein−lipid interactions, we examined the changes in a soluble, membrane-free construct of HA2 (SHA2, aa 33−127). The SHA2 construct lacks the first 32 amino acids in the N-terminal region, including the essential fusion peptide, and does not bind to the membrane. S113C showed considerable broadening at pH 5 in the SHA2 construct (Figure 5B) as did the same position in FHA2 (Figure 5A). In addition, the reversibility of this change for SHA2 was identical to that of FHA2 shown in Figure 5.

A second mutant in SHA2 at residue 64 was used as a control to verify whether the pH-dependent change was localized in the kinked region of SHA2 as it was in FHA2. EPR line shapes for this spin-labeled mutant did not show an appreciable change with pH (Figure 5B). This is precisely what we observed for membrane-bound FHA2 at position 64 *(17)*. Thus, it would appear that the SHA2 construct behaves like FHA2 and demonstrates that changes in the kinked region are independent of vesicles.

DISCUSSION

An important stride in understanding HA-mediated membrane fusion was made by establishing a low-pH crystal structure of soluble HA2 *(12)*. However, this structure on its own leaves several intriguing questions unanswered. Paramount among these questions is: How does HA2 assemble so as to mediate membrane apposition and fusion? Our goal was to shed light on the events of HA-mediated membrane fusion after the initial low-pH-induced conformational change of HA2.

In this study, we expressed an HA2 construct (aa 1−127, FHA2) which is a trimer *(17)* and contains all four major structural components from the pH 7 structure of the HA2 ectodomain (Figure 1). Our EPR observations strongly indicate that the kinked region is involved in low-pH-induced protein−protein interactions. EM data of vesicles carrying FHA2 during a pH 7 to pH 5 change (Figure 4) suggest that FHA2 promotes a reversible, pH-dependent clustering of vesicles. Furthermore, the lack of a pH-dependent structural change in the middle of the long coiled-coil or in fusion peptide *(17, 16)* supports the hypothesis that the kinked region is primarily responsible for pH-dependent protein−protein interactions. Additionally, the kink region of one trimer makes crystal contacts with the kink of another trimer in the low-pH crystal structure (D. Wiley, personal communication), indicating that the kinked regions do have affinity for one another at pH 5. The nature of this protein−protein interaction is not fully understood (e.g., which residues are in contact). Instead, this study provides grounds for a more detailed analysis of how the kinked regions of HA and other related proteins affect membrane fusion.

Implications for Recent Fusion Models. The structure of membrane-bound HA2 and the low-pH-induced interactions at the kinked region provide insights into HA-mediated membrane fusion. In the following section, we will discuss the implications of our results on various classes of fusion models.

The first type of membrane fusion model is based on the interaction of fusion peptide with the membrane. Indeed, some reports imply that at high concentrations, synthetic peptides can induce fusion *(26)*. However, recently it has been shown that membrane-anchored fusion peptides without the coiled-coil stem do not cause membrane fusion, although they do disrupt the membrane at increasing concentrations *(27)*. With this in mind, we propose that the interactions between HA2 trimers via their kinked loops might be essential for increasing the local concentration of fusion peptides, thus facilitating membrane disruption and the formation of a fusion pore.

A second model of fusion involves the concerted activity of several trimers. First an initial hemifusion or full fusion pore is formed by the assembly of a few HA trimers *(28, 29)*. This assembly of trimers could be mediated by protein−protein interactions in their kinked loops. Furthermore, a mechanism of inactivation has been reported based on a lateral overaggregation of HA *(30)*. The interactions of HA2 kinks in the absence of a target membrane could promote an irreversible lateral aggregation through interactions between hydrophobic regions on neighboring HA2 complexes. Indeed, we have observed a less reversible change in turbidity when vesicles carrying FHA2 were exposed to pH 5 for more

than 30 min at 37 °C (unpublished data). This shows that the protein−protein interactions in the kinked region could be an initial step of irreversible lateral aggregation.

A third class of fusion models suggests that each HA trimer interacts individually with the membrane through a splay−insertion mechanism. This model was proposed in a recent EPR study which suggested that a portion of the long coiled-coil nearest to the fusion peptide inserts into the target membrane *(31)*. Further evidence for this model came from a quick-freezing electron microscopy study where single HA trimers appear to cause microprotrusions in the apposing membranes *(32)*. A key question left unanswered in this EM study might be addressed by our findings. Each membrane microprotrusion is presumed to contain one protein particle, 100 Å in diameter, which moves out of the fusion region through some unknown mechanism as fusion begins. The size and location of these protein particles agree well with the topology and structure of the membrane-bound fusion peptide region (*16*). Our current study provides a mechanism that would allow the imbedded fusion peptides and connecting protein to move away from the fusion site at the onset of fusion. Lateral protein−protein interactions could draw an interacting trimer away from the microprotrusion.

A final example of a fusion model is one based on the tilting of HA trimers *(1)*. This tilting could be assisted by the specific interactions between the kinked loops of neighboring trimers. Such a tilt at pH 5 was observed by Tamm and co-workers *(33)* and was also shown to be reversible *(34)*, which parallels the reversibility of kink interactions observed in this study.

The importance of the kinked region comes as no surprise given the recent evidence that the kinked structural motif is present in many other viral spike proteins, including gp41 of HIV *(13)* and the transmembrane (TM) subunit of Moloney murine leukaemia virus (Mo-MLV) *(15)*. Our findings will help to pinpoint which regions in HA2 are most responsible for the pH-dependent fusion process. Synthetic peptides derived from the bunching kink region may be developed in an effort to better understand and perhaps block the infection mechanism of the influenza virus.

ACKNOWLEDGMENT

We thank Dr. B. G. Han for his technical support and valuable discussion regarding electron microscopy, and Peter Loc and Edward Lee for their work in FHA2 expression and purification.

REFERENCES

1. White, J. M. (1992) *Science 258*, 917−924.
2. Stegmann, T., Doms, R. W., and Helenius, A. (1989) *Annu. Rev. Biophys. Biophys. Chem. 18*, 187−211.
3. Matlin, K. S., Reggio, H., Helenius, A., and Simons, K. (1981) *J. Cell Biol. 91*, 601−613.
4. Skehel, J. J., Bayley, P. M., Brown, E. B., Martin, S. R., Waterfield, M. D., White, J. M., Wilson, I. A., and Wiley, D. C. (1982) *Proc. Natl. Acad. Sci. U.S.A. 79*, 968−972.
5. Wiley, D. C., and Skehel, J. J. (1987) *Annu. Rev. Biochem. 56*, 365−394.
6. Stegmann, T., and Helenius, A. (1993) in *Viral Fusion Mechanisms* (Bentz, J., Ed.) pp 89−111, CRC Press, Inc., Boca Raton, FL.
7. Wilson, I. A., Skehel, J. J., and Wiley, D. C. (1981) *Nature (London) 289*, 366−373.
8. Doms, R. W., and Helenius, A. (1986) *J. Virol. 60*, 833−839.
9. Stegmann, T., White, J. M., and Helenius, A. (1990) *EMBO J. 9*, 4231−4241.
10. Stegmann, T., Delfino, J. M., Richards, F. M., and Helenius, A. (1991) *J. Biol. Chem. 266*, 18404−18410.
11. Carr, C. M., and Kim, P. S. (1993) *Cell 73*, 823−832.
12. Bullough, P. A., Hughson, F. M., Skehel, J. J., and Wiley, D. C. (1994) *Nature (London) 371*, 37−43.
13. Chan, D. C., Fass, D., Berger, J. M., and Kim, P. S. (1997) *Cell 89(2)*, 263−273.
14. Weissenhorn, W., Dessen, A., Harrison, S. C., Skehel, J. J., and Wiley, D. C. (1997) *Nature 387*, 426−430.
15. Fass, D., Harrison, S. C., and Kim, P. S. (1996) *Nat. Struct. Biol. 3*, 465−469.
16. Macosko, J. C., Kim, C.-H., and Shin, Y.-K. (1997) *J. Mol. Biol. 267*, 1139−1148.
17. Kim, C.-H., Macosko, J. C., Yu, Y. G., and Shin, Y.-K. (1996) *Biochemistry 35*, 5359−5365.
18. Sambrook, J., Fritsch, E. F., and Maniatis, T. (1989) in *Molecular Cloning*, pp A.1−A.3, Cold Spring Harbor Laboratory Press, Plainview, NY.
19. Kunkel, T. A. (1985) *Proc. Natl. Acad. Sci. U.S.A. 82*, 488−492.
20. Rabenstein, M., and Shin, Y.-K. (1995) *Biochemistry 34*, 13390−13397.
21. Holloway, P. W. (1973) *Anal. Biochem. 53*, 304−308.
22. Altenbach, C., Greenhalgh, D. A., Khorana, H. G., and Hubbell, W. L. (1994) *Proc. Natl. Acad. Sci. U.S.A. 91*, 1667−1671.
23. Altenbach, C., Yang, K., Farrens, D. L., Farahbakhsh, Z. T., Khorana, H. G., and Hubbell, W. L. (1996) *Biochemistry 35*, 12470−12478.
24. Yu, Y. G., Thorgeirsson, T. E., and Shin, Y.-K. (1994) *Biochemistry 33*, 14221−14226.
25. Hubbell, W. L., and Altenbach, C. (1994) *Site-directed spin labeling of membrane proteins* in *Membrane Protein Structure: Experimental Approaches* (White, S., Ed.) Oxford University Press, New York.
26. Lear, J. D., and DeGrado, W. F. (1987) *J. Biol. Chem. 262*, 6500−6505.
27. Bailey, A. L., Monck, M. A., and Cullis, P. R. (1997) *Biochim. Biophys. Acta 1324(2)*, 232−244.
28. Danieli, T., Pelletier, S. L., Henis, Y. I., and White, J. M. (1996) *J. Cell Biol. 133*, 559−569.
29. Blumenthal, R., Sarker, D. P., Durell, S., Howard, D. E., and Morris, S. J. (1996) *J. Cell Biol. 135*, 63−71.
30. Gutman, O., Danieli, T., White, J. M., and Henis, Y. I. (1993) *Biochemistry 32*, 101−106.
31. Yu, Y. G., King, D. S., and Shin, Y.-K. (1994) *Science 266*, 274−276.
32. Kanaseki, T., Kawasaki, K., Murata, M., Ikeuchi, Y., and Ohnishi, S. (1997) *J. Cell Biol. 137*, 1041−1056.
33. Tatulian, S. A., Hinterdorfer, P., Baber, G., and Tamm, L. K. (1995) *EMBO J. 14(22)*, 5514−5523.
34. Tatulian, S. A., and Tamm, L. K. (1996) *J. Mol. Biol. 260-(30)*, 312−316.

BI971982W